DRAFT VERSION MAY 6, 2013
Preprint typeset using LaTeX style emulateapj v. 12/01/06

KINEMATICS PAPER

JESSICA L. EVANS,[1] CHRISTOPHER W. CHURCHILL,[1] MICHAEL T. MURPHY,[2], AND NIKOLE M. NIELSEN[1]

Draft version May 6, 2013

ABSTRACT

Subject headings: quasars: absorption lines

1. INTRODUCTION

In Evans et al. (2013) (hereafter, Paper I) we introduced our high resolution, high signal-to-noise Mg II absorber sample and presented our results for equivalent widths, kinematic extents, kinematic systems, and flux decrements as a function of velocity, as well as the evolution of these properties.

In this paper we discuss and analyze the results of our Voigt profile (VP) decomposition models, which were plotted with our Mg II absorption profile data in Paper I. As in the previous work, we here adopt the terms "weak" and "strong" to refer to absorbers having 0.02 Å $\leq W_r < 0.3$ Å and $W_r \geq 0.3$ Å, respectively, where W_r is the rest frame equivalent width of the Mg II λ2796 transition.

2. DATA

We have analyzed 252 high resolution, high signal-to-noise High Resolution Echelle Spectrometer (HIRES) and Ultraviolet and Visual Echelle Spectrograph (UVES) quasar spectra obtained from the Keck and Very Large Telescope (VLT) observatories, respectively. The Mg II λ2796 redshift coverage of the survey is $0.1 < z < 2.6$. Details of the reduction procedure as well as the coverage, sensitivity, characteristics, and possible sources of bias of the spectra can be found in Paper I, which also contains an in-depth discussion of the search algorithm and criteria for identifying Mg II doublets; however, we review the information here. The λ2796 feature is required to have a significance level of at least $5\,\sigma$, and the corresponding λ2803 feature at least $3\,\sigma$. In total, 469 Mg II $\lambda\lambda 2796, 2803$ systems were identified, but after making a quality cut based on signal-to-noise (Paper I), 422 systems remained to comprise our sample. Our Mg II λ2796 rest equivalent width sample ranges from 0.006 Å to 6.23 Å. The absorbing redshifts span the range $0.19 \leq z \leq 2.55$, with a mean of 1.18.

For each Mg II $\lambda\lambda 2796, 2803$ system in our final sample, absorption features were measured and VP models were fit for 13 transitions derived from five different elements: Mg II λ2796 and λ2803; Mg I λ2853; Fe II λ2344, λ2374, λ2383, λ2587, and λ2600; Ca II λ3935 and λ3970; and Mn II λ2577, λ2594, and λ2606. Each system's absorption profiles for all the transitions for which VP components were modeled are shown in the online version of Paper I; six examples are shown in order of increasing equivalent width in Figures 1.1 and 1.2.

3. VOIGT PROFILE FITTING

In order to extract as much information as possible from the Mg II systems in our sample, we utilized VP fitting in addition to the directly measured quantities discussed in Paper I. The Voigt profile takes into account two absorption line broadening mechanisms: the natural linewidth, which results from Heisenberg uncertainty, and Doppler broadening, which is a result of the thermal and/or turbulent motions of the gas. The natural linewidth is characterized by a Lorentzian and the Doppler, or thermal, broadening by a Gaussian. Their convolution results in the Voigt profile. Complex absorption systems can be decomposed into individual Voigt profiles, with each model component yielding column density, temperature, and velocity information. Further details of the Voigt function are discussed in the Appendix.

The VP fitting philosophy and modeling process are explained in the following sections; an example of the results for an Mg II system is listed in Table 1. Column (1) lists the velocity of the cloud and (2)–(11) list the column densities N and Doppler parameters b of the five analyzed ions, Mg II, Fe II, Mg I, Mn II, and Ca II. Column densities listed as being less than or equal to some value represent upper limits (see § 3.2). Example fits are shown plotted over the data in Figures 1.1 and 1.2. Systems that are present in both our sample and either Churchill (1997) or Churchill et al. (2003) have been refit for uniformity.

3.1. *Fitting Philosophy*

The ionization potentials of the five ions included in the fit are all close to the H I potential of 13.59 eV. Their absorption is therefore all assumed, for the purpose of VP fitting, to arise in the same spatial extent of gas, and to contain the same velocity structure. The Mg I and Ca II potentials are both below that of H I at 7.65 eV and 11.87 eV, respectively, while those of Mg II, Fe II, and Mn II are all slightly above at 15.04 eV, 16.19 eV, and 15.63 eV, respectively. This spread does mean, however, that the ionization structure of a given parcel of gas might be different for different ions. Inasmuch as this difference affects velocity structure, our assumption of parallel kinematics across ions may not always be completely correct.

Another consideration in VP decomposition is how to fit the Doppler b parameter across ions. For our study, we have chosen to let the user input whether to constrain this parameter as 100% turbulent or 100% thermal. In the former case, the b parameter will be fit such that the result is identical for all ions within a given velocity component; in the latter case, it will vary as the ratio of the square root of the atomic masses. The default condition used was turbulent; departures from this are noted in the descriptions of individual systems in the Supplement. The systems were fit under the thermal condition if a satisfactory fit could not be achieved using the turbulent condition.

The overarching VP fitting philosophy used for this study was to fit the Mg II systems using as few components as possible while still achieving a robust fit in which all components were statistically significant. In addition, VP modeling by nature requires the assumption of isothermal components that

[1] New Mexico State University, Las Cruces, NM 88003
[2] Centre for Astrophysics and Supercomputing, Swinburne University of Technology, Hawthorn, Melbourne, VIC 3122, Australia

TABLE 1
VOIGT PROFILE FITTING RESULTS

	Mg II		Fe II		Mg I		Mn II		Ca II	
v (km s^{-1})	N (cm^{-2})	b (km s^{-1})	N (cm^{-2})	b (km s^{-1})	N (cm^{-2})	b (km s^{-1})	N (cm^{-2})	b (km s^{-1})	N (cm^{-2})	b (km s^{-1})
J012417-374423 z_{abs} = 1.173635										
–0.91	11.64±0.027	6.92±0.672	≤ 10.62	···	≤ 10.55	···	≤ 10.61	···	···	···
J101447+430031 z_{abs} = 2.042606										
–98.07	12.11±0.018	3.73±0.334	≤ 10.75	···	···	···	≤ 10.83	···	···	···
11.34	11.91±0.030	5.76±0.674	≤ 10.84	···	···	···	11.29±0.249	5.76±0.674	···	···
29.01	11.35±0.105	4.52±2.287	≤ 10.78	···	···	···	≤ 10.87	···	···	···
45.26	11.33±0.107	4.87±2.386	≤ 10.78	···	···	···	≤ 10.96	···	···	···
J123200-022404 z_{abs} = 0.756903										
–9.28	12.75±0.070	6.24±0.513	11.58±0.171	6.24±0.513	≤ 10.72	···	···	···	···	···
2.42	13.33±0.023	6.73±0.230	12.30±0.034	6.73±0.230	10.87±0.084	6.73±0.230	···	···	···	···
30.47	11.77±0.039	9.08±1.177	11.23±0.339	9.08±1.177	≤ 10.78	···	···	···	···	···
J110325-264515 z_{abs} = 1.202831										
–79.98	12.34±0.001	5.84±0.000	11.80±0.020	5.84±0.000	≤ 11.56	···	≤ 10.47	···	≤ 10.15	···
–65.77	12.21±0.008	5.12±0.000	11.58±0.037	5.12±0.000	≤ 11.63	···	≤ 10.47	···	≤ 10.10	···
–33.23	12.19±0.007	5.85±0.000	11.49±0.030	5.85±0.000	≤ 11.67	···	≤ 10.47	···	≤ 10.07	···
–22.33	12.02±0.076	3.08±0.411	11.50±0.056	3.08±0.411	≤ 11.61	···	≤ 10.37	···	≤ 9.97	···
–9.16	12.84±0.005	7.33±0.013	12.14±0.012	7.33±0.013	≤ 10.49	···	≤ 10.54	···	≤ 10.15	···
5.80	15.06±0.017	2.67±0.013	12.55±0.005	2.67±0.013	11.29±···[a]	2.67±0.013	≤ 10.37	···	≤ 10.00	···
52.08	12.57±0.004	4.02±0.013	11.70±0.026	4.02±0.013	≤ 11.62	···	≤ 10.43	···	≤ 10.07	···
61.25	11.13±0.067	6.72±0.779	≤ 10.50	···	≤ 11.73	···	≤ 10.51	···	≤ 10.15	···
86.15	11.70±0.018	7.36±0.448	11.07±0.122	7.36±0.448	≤ 11.58	···	≤ 10.54	···	≤ 10.17	···
J110325-264515 z_{abs} = 1.838689										
–126.13	11.86±0.009	9.10±0.275	10.92±0.103	9.10±0.275	≤ 10.44	···	11.48±0.025	9.10±0.275	···	···
–103.14	12.41±0.002	6.12±0.058	11.54±0.022	6.12±0.058	≤ 10.38	···	10.99±0.061	6.12±0.058	···	···
–50.66	12.61±0.005	7.69±0.096	11.87±0.013	7.69±0.096	10.54±0.055	7.69±0.096	10.56±0.179	7.69±0.096	···	···
–38.04	12.26±0.009	4.04±0.113	11.64±0.019	4.04±0.113	≤ 10.45	···	≤ 10.29	···	···	···
–15.10	13.50±0.005	6.62±0.034	12.89±0.002	6.62±0.034	11.33±0.011	6.62±0.034	10.75±0.108	6.62±0.034	···	···
–3.50	12.69±0.052	1.61±0.072	11.80±0.021	1.61±0.072	10.61±0.045	1.61±0.072	11.01±0.049	1.61±0.072	···	···
4.58	12.95±0.003	5.66±0.070	12.55±0.004	5.66±0.070	10.75±0.036	5.66±0.070	11.07±0.053	5.66±0.070	···	···
22.46	13.82±0.009	5.21±0.021	13.19±0.002	5.21±0.021	11.50±0.007	5.21±0.021	11.23±0.034	5.21±0.021	···	···
38.69	11.95±0.011	1.50±0.095	11.42±0.029	1.50±0.095	10.23±0.094	1.50±0.095	10.53±0.143	1.50±0.095	···	···
47.82	12.53±0.004	3.16±0.067	12.48±0.003	3.16±0.067	10.74±0.034	3.16±0.067	10.57±0.140	3.16±0.067	···	···
58.56	12.57±0.005	2.87±0.063	12.41±0.004	2.87±0.063	10.65±0.040	2.87±0.063	≤ 10.25	···	···	···
69.13	12.41±0.004	4.41±0.085	11.92±0.011	4.41±0.085	10.30±0.086	4.41±0.085	≤ 10.30	···	···	···
J035405-272421 z_{abs} = 1.405188										
–160.39	12.55±0.017	10.91±0.560	12.33±0.029	10.91±0.560	···	···	≤ 11.04	···	···	···
–141.33	12.64±0.016	5.63±0.278	12.50±0.019	5.63±0.278	···	···	10.99±0.319	5.63±0.278	···	···
–113.89	13.35±0.037	6.36±0.163	13.37±0.011	6.36±0.163	···	···	10.83±0.488	6.36±0.163	···	···
–99.75	13.38±0.229	2.78±0.215	13.21±0.024	2.78±0.215	···	···	10.98±0.300	2.78±0.215	···	···
–91.97	12.52±0.261	2.33±1.009	12.51±0.082	2.33±1.009	···	···	10.52±0.902	2.33±1.009	···	···
–80.97	13.74±0.077	25.95±3.388	13.32±0.077	25.95±3.388	···	···	11.64±0.190	25.95±3.388	···	···
–56.41	13.71±0.232	11.32±3.223	13.46±0.232	11.32±3.223	···	···	≤ 10.95	···	···	···
–45.25	13.59±0.205	6.76±0.447	13.54±0.097	6.76±0.447	···	···	11.53±0.118	6.76±0.447	···	···
–21.63	13.19±0.072	5.87±0.528	12.89±0.066	5.87±0.528	···	···	10.67±0.643	5.87±0.528	···	···
–1.43	14.53±0.045	10.13±0.721	14.30±0.045	10.13±0.721	···	···	11.92±0.072	10.13±0.721	···	···
24.38	15.09±0.051	13.06±1.612	14.86±0.051	13.06±1.612	···	···	12.57±0.051	13.06±1.612	···	···
38.83	14.65±0.105	4.56±0.928	14.42±0.105	4.56±0.928	···	···	11.94±0.160	4.56±0.928	···	···
51.57	15.60±0.398	1.83±0.241	15.38±0.398	1.83±0.241	···	···	11.97±0.037	1.83±0.241	···	···
65.15	15.10±0.051	7.02±0.091	14.21±0.009	7.02±0.091	···	···	12.13±0.026	7.02±0.091	···	···
94.62	12.98±0.010	6.47±0.163	12.53±0.014	6.47±0.163	···	···	≤ 10.95	···	···	···
125.71	12.23±0.040	14.33±1.809	11.79±0.099	14.33±1.809	···	···	11.24±0.251	14.33±1.809	···	···
148.04	13.64±0.060	4.44±0.134	13.25±0.012	4.44±0.134	···	···	≤ 10.96	···	···	···
159.68	13.33±0.037	8.97±0.426	12.68±0.034	8.97±0.426	···	···	≤ 10.95	···	···	···

Notes. Results for the systems shown in Figures 1.1 and 1.2. Table 1 is published in its entirety in the electronic edition of the Journal. A portion is shown here for guidance regarding its form and content.

[a] Quantity was not well constrained.

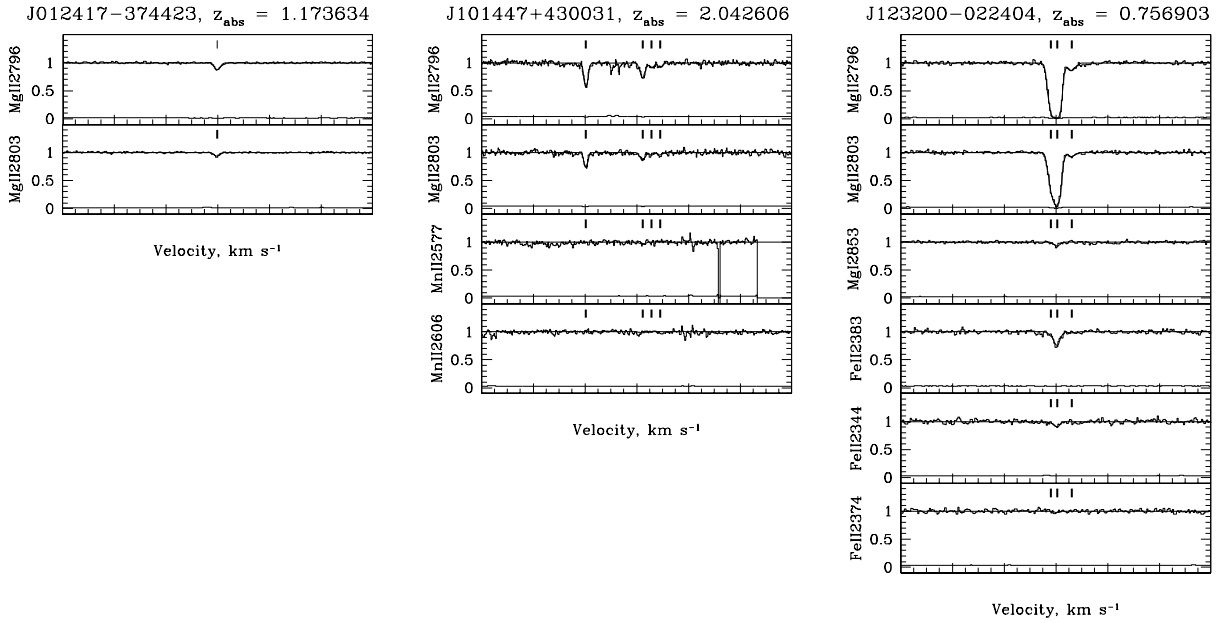

FIG. 1.1.— System absorption profiles. The VP models are superimposed; ticks indicate the component centroids.

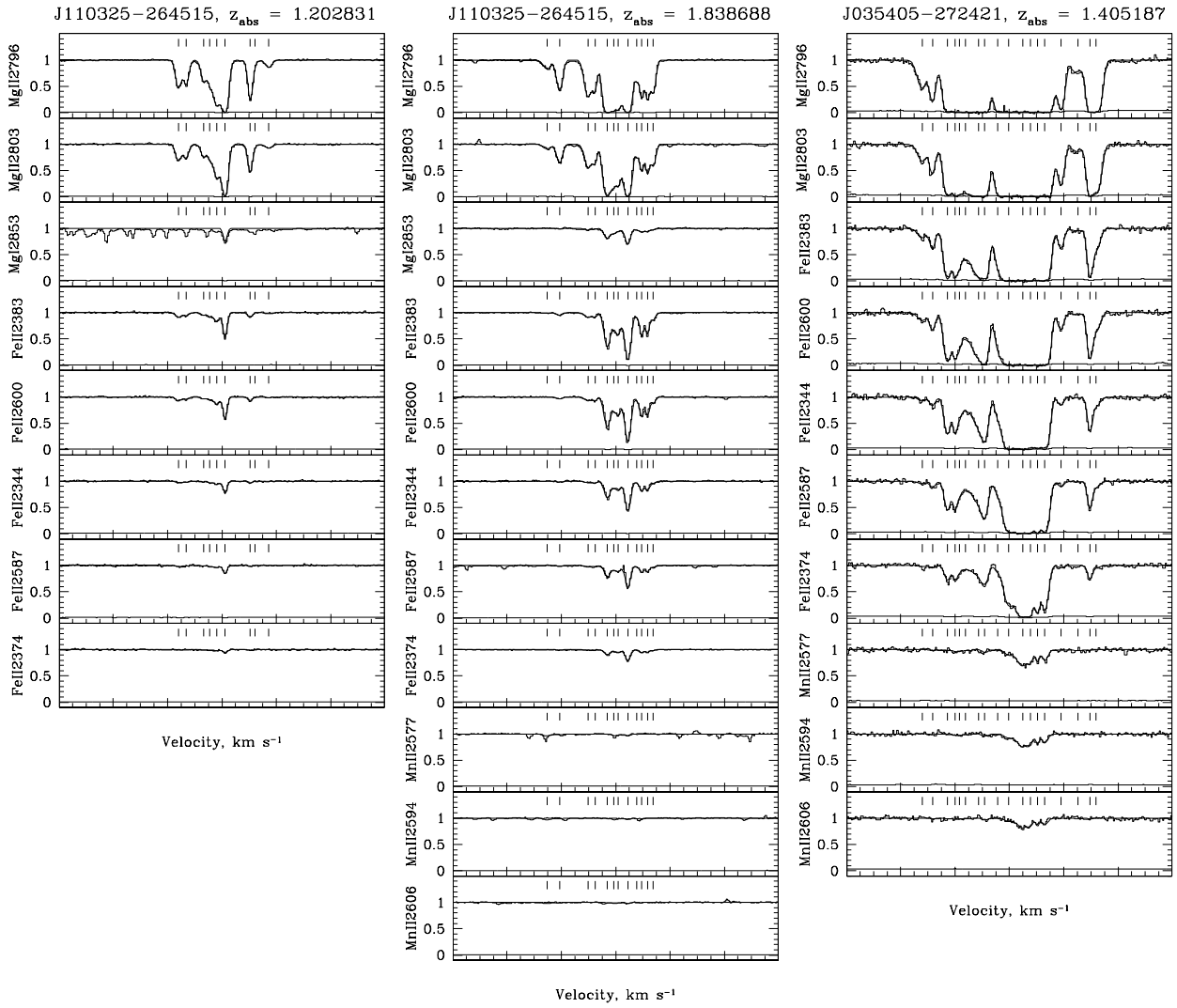

FIG. 1.2.— Same as Figure 1.1.

occupy distinct points in velocity space.

3.2. *Fitting Procedure*

Using the graphical interactive program IVPFIT, which is an improved version of PROFIT (Churchill 1997), an initial model of an absorption system's VP components is created and adjusted to fit the data as closely as possible. The velocity, Doppler parameter, and column density of each component are input by the user.

The least squares fitter MINFIT (Churchill 1997), using this initial model, iteratively eliminates all statistically insignificant components and adjusts the remaining components until the least squares fit is achieved. This process is discussed below and illustrated in Figure 2. The velocities, column densities, Doppler parameters, and temperatures are calculated for each VP component. MINFIT utilizes the spectral information from all available transitions to constrain these parameters. The velocity of a given component is constrained to be the same across all transitions. The column density is constrained to be the same across all transitions of a given ion. Finally, the Doppler parameter can be set by the user to either vary thermally across ions or to remain constant across all ions, as discussed in § 3.1.

Over Mg II fitting regions that were saturated but for which the Fe II ion retained good column density constraints, a special feature of MINFIT was employed. The user can specify velocity ranges in which the code enforces a $\log N$(Mg II) to $\log N$(Fe II) relationship determined empirically by Churchill et al. (2003), $\log N(\mathrm{Mg\,II}) = 1.37 \times \log N(\mathrm{Fe\,II}) - 0.41$, instead of allowing the column densities of the two ions to be fit independently. This prevents unphysical Mg II to Fe II column density ratios.

In many systems, one or more transitions may be contaminated over portions of the velocity extent by either bad pixels, noisy pixels, or spurious features, all of which have no corroborating absorption in other transitions. In these cases, MINFIT allows the user to interactively mask out regions or individual pixels from the fit. Once this has been done, the code will consider any masked regions of a transition to contain no data and thus to contribute no information to the fit.

MINFIT fits three free parameters for each VP component: the column density, the Doppler parameter, and the redshift of the component center. The fitting process and uncertainty calculations are described in detail in Churchill (1997). When

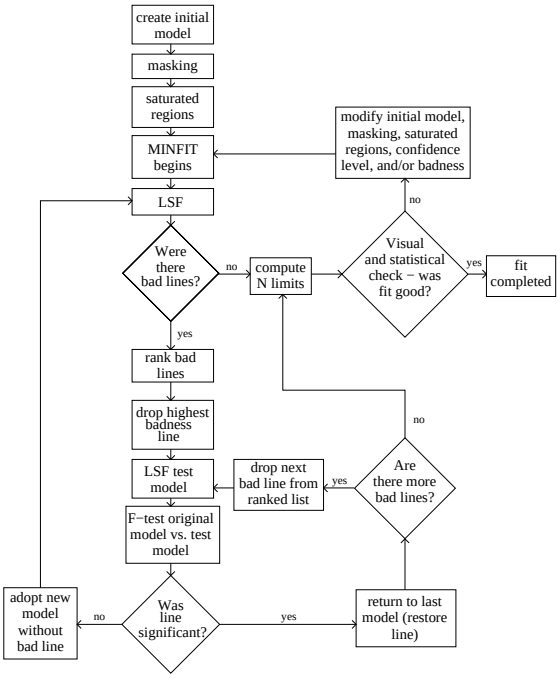

FIG. 2.— The Voigt profile modeling process.

there are multiple kinematic subsystems, the redshift region for each is fit separately. All available transitions within a redshift region are fit simultaneously.

As illustrated in Figure 2, MINFIT is started after the initial model is created and any saturated or masked regions have been defined. The program performs the first χ^2 minimization of the first redshift region and then begins the process of determining which components to reject from the model of that region. The badness, or fractional error, of each Mg II component is calculated,

$$\text{badness} = \left[\left(\frac{dN}{N}\right)^2 + \left(\frac{db}{b}\right)^2 + \left(\frac{dz}{z}\right)^2\right]^{1/2}, \qquad (1)$$

where N is the column density, b is the Doppler parameter, and z is the absorption redshift. All components exceeding the user input badness ("bad" components or lines) are ranked. The component with the highest badness is removed from the model and this new "test" model is least squares fit (LSF). Next an F-test is performed comparing the LSFs of the two models; the original model (i.e. containing the bad component) is retained if the resulting confidence level equals or exceeds the user input confidence level. Then the next highest badness component is dropped from the model and the χ^2 minimization process is repeated for this new test model. Otherwise, if the required confidence level was not met, the test model (i.e. with the bad component removed) replaces the original model and the χ^2 minimization process is begun from the beginning (i.e. a new list of bad components, if any, is created). This process is continued until either there are no bad components or any bad components deemed significant to the fit are retained after F-testing.

Once the model has converged for a redshift region, the program moves on to the next region and the LSF process is started again until all regions have been modeled. The code employs a badness of 1.5 and a confidence level of 0.97; on a case-by-case basis, however, these parameters may be altered if it is determined that the final model was unsatisfactory using the default values. These exceptions are noted in the descriptions of individual systems in (REFER TO ONLINE VERSION SUPP MATERIAL OF PAPER I).

When all regions have been modeled, column density component upper limits are computed. This is done whenever Mg II was modeled but the component was deemed not present in another ion, i.e. the data was consistent with the continuum.

4. RESULTS

4.1. *Number of VP Components*

The left panel of Figure 3 shows the distribution of the number of VP components in each system. The dotted line shows the weak subsample ($W_r(2796) < 0.3$ Å), the dashed line the strong subsample ($W_r(2796) \geq 0.3$ Å), and the shaded area the full sample. The weak systems were modeled with an average of 2.7 components, the strong systems 10.3 components, and the full sample 7.1 components.

Churchill et al. (2003), in modeling simulated complex Mg II absorption systems, found that $\sim 30\%$ of VP components were not recovered. If this holds true in our sample, it would mean that the actual mean numbers of components are $\sim 43\%$ higher than what was modeled, implying an actual average number of components for the full sample of ~ 10.2, and for the weak and strong subsamples ~ 3.9 and ~ 14.7, respectively.

The Mg II λ2796 system equivalent widths are plotted as a function of the number of VP components in the system in the right panel of Figure 3. Gray circles indicate weak systems and black circles indicate strong systems. A linear fit to the full sample resulted in a slope of 0.116 ± 0.003 Å cloud^{-1}. The slope found by Churchill (1997) for a sample of 36 Mg II systems at the same spectral resolution as this study was 0.076 ± 0.004 Å cloud^{-1}. A lower resolution (~ 30 km s^{-1}) study by Petitjean & Bergeron (1990) for a sample of 10 Mg II systems yielded a steeper slope of 0.35 Å cloud^{-1}. The W_r - N_{VP} relationship is strongly affected by the resolution as well as by the signal-to-noise ratio (SN), since higher SN (Churchill 1997) as well as higher resolution allow more components to be recovered in the VP decomposition.

4.2. *Column Density Distribution*

The column density distribution of Mg II VP components can be studied in a manner similar to that of the equivalent widths and modeled using a power law fit. This quantity can sometimes be more revealing because, though more difficult to obtain because of the need to VP fit, it can somewhat account for saturation and therefore the differing sizes of systems that lie on the flat part of the curve of growth.

VP analysis of our full sample of Mg II systems yields the component column density distribution shown in Figure 4. The 422 Mg II systems of our sample yielded 2,989 VP components. The shaded area indicates the region of partial completeness determined by the simulations of Churchill et al. (2003). That study found that the 90% completeness levels for unblended and blended lines were log N(Mg II) = 11.6 cm^{-2} and 12.4 cm^{-2}, respectively, for spectra having a 5 σ equivalent width sensitivity of W_r = 0.02 Å. "Completeness level" refers to the percentage of simulated components of a given column density recovered during VP analysis. Our distribution peaks in the bin centered at 11.25 cm^{-2}; however, the turnover at lower column densities is believed to be caused by incompleteness.

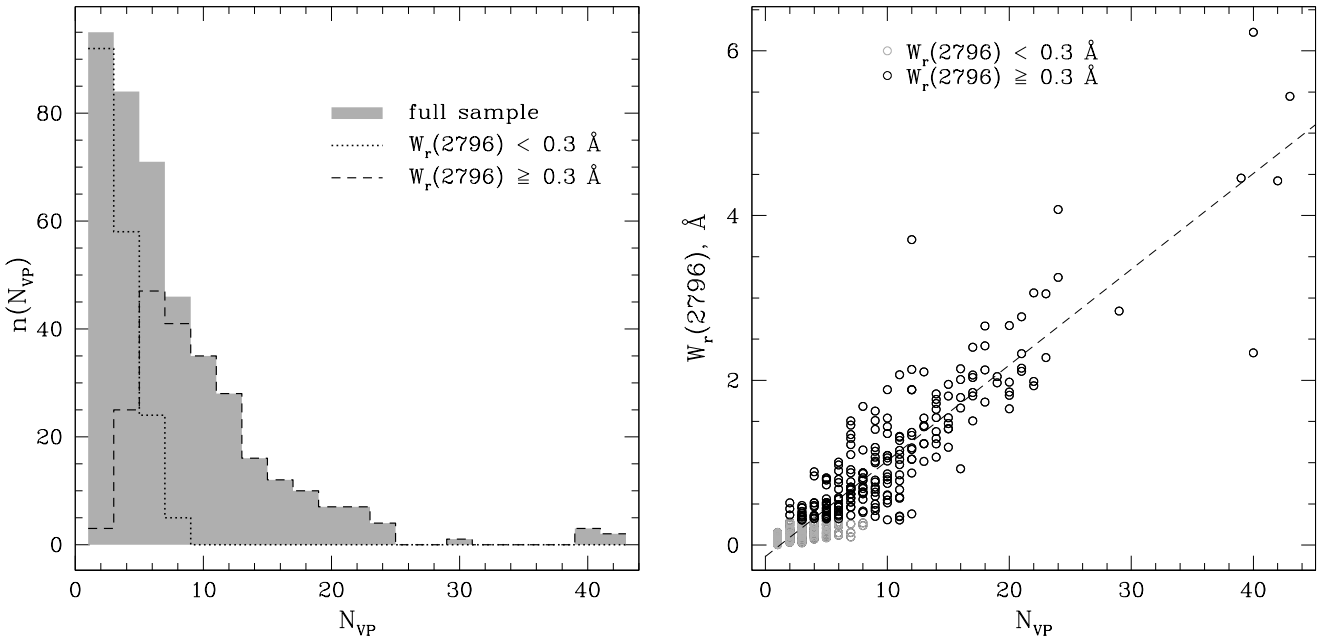

FIG. 3.— At left, the distribution of the number of VP components N_{VP} for $W_r(2796) < 0.3$ Å, $W_r(2796) \geq 0.3$ Å, and the full sample. At right, the system equivalent width versus N_{VP} for weak and strong Mg II systems. The dotted line indicates a linear fit to the full sample; the slope is 0.116 ± 0.003 Å cloud^{-1}.

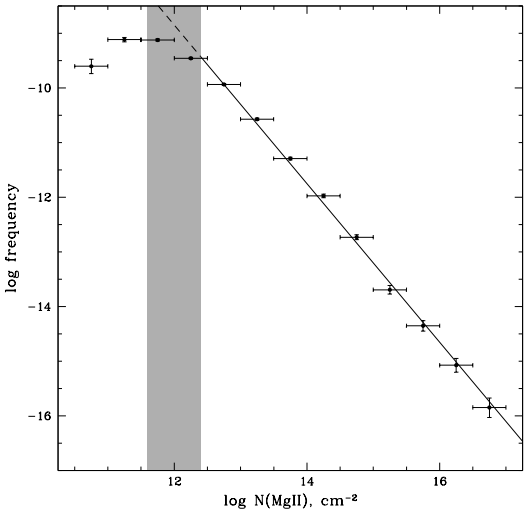

FIG. 4.— The logarithmic VP column density distribution. The shaded area indicates the region of partial completeness (see text). The solid sloped line plots the power law maximum likelihood fit, which was performed on all VP column densities of log N(Mg II) > 12.4 cm^{-2} and which resulted in a slope of $\delta = 1.45 \pm 0.01$. The dashed sloped line shows the fit extended to lower column densities for comparison with the data.

The column density distribution can be fit by a power law, which takes the form

$$f(N) = CN^{-\delta}, \quad (2)$$

where $f(N)$ is the number of clouds with column density N per unit column density, C is a normalization constant and δ is the power law slope. The maximum likelihood method was used to obtain the power law fit to the unbinned data. The fit was performed only on column densities above the region of partial completeness (log N(Mg II) > 12.4 cm^{-2}) so as not to skew it to an artificially shallower slope. Our result for the power law slope was $\delta = 1.45 \pm 0.01$. In a study of 14 Mg II systems containing 33 VP components, Petitjean & Bergeron (1990) obtained a significantly shallower slope of $\delta = 1.0 \pm 0.1$, although their spectral resolution was lower. In a study with comparable resolution to ours, Churchill et al. (2003) obtained $\delta = 1.59 \pm 0.05$ by fitting their sample of 175 VP components in 23 Mg II systems. This result agrees closely with our column density distribution fit.

4.3. *Doppler Parameter Distribution*

The Mg II Doppler b parameter distribution of VP components is shown in Figure 5. The median Doppler parameters

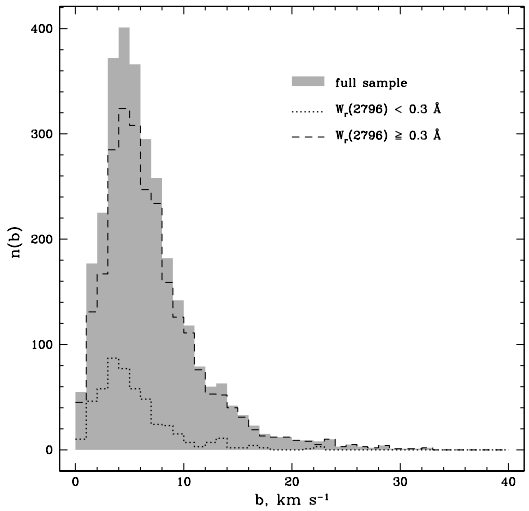

FIG. 5.— The Doppler parameter distribution of VP components for $W_r(2796) < 0.3$ Å, $W_r(2796) \geq 0.3$ Å, and the full sample.

and standard deviations are 4.5 ± 3.5 km s^{-1}, 6.0 ± 4.5 km s^{-1}, and 5.7 ± 4.4 km s^{-1} for the weak, strong, and full samples, respectively. Churchill (1997) found a median Doppler parameter of ~ 3.5 km s^{-1} in a study of 48 Mg II systems and

Churchill et al. (2003) found 5.4 ± 4.3 in a study of 23 Mg II systems; in both cases the data were of comparable quality. Petitjean & Bergeron (1990) found in their study of 14 Mg II systems that the *b* distribution peaked between 10 and 15 km s^{-1}; however, they were limited by an inferior spectral resolution of 30 km s^{-1} and noted that this significantly distorted the observed distribution. The authors' high Doppler parameter results led them to conclude that a significant turbulent component was broadening the lines, since a purely thermal *b* would correspond to temperatures too high for Mg II to exist.

Based on simulations (Churchill et al. 2003), our observed distribution peak, the bin centered at 4.5 km s^{-1} for the full sample, is likely $\sim$1-2 km s^{-1} too high relative to the true distribution. In addition, the distribution tail at high *b* values has been shown in these simulations to be an artifact of component blending. As mentioned in § 4.1, $\sim 30\%$ of simulated components are not recovered in the VP decomposition for our spectral quality. As a result, some *b* parameters in the observed distribution are too broad compared to the true distribution due to compensation for loss of some components, e.g. in saturated profiles where VP component parameters are not well constrained.

If the Doppler broadening is assumed to be purely thermal, then the observed *b* parameter distribution medians correspond to gas temperatures of $\sim 30,000$ K, $\sim 53,000$ K, and $\sim 47,000$ K for the weak, strong, and full samples, respectively. However, applying the 1-2 km s^{-1} correction to the *b* parameter would produce, in the case of the full sample, a median temperature of $\sim 20,000-32,000$ K; in the weak sample, $\sim 9,000-18,000$ K; and in the strong sample, $\sim 23,000-37,000$ K. Figure 5 reveals that the high *b* tail of the distribution is heavily dominated by strong systems, leading to the higher temperature prediction for this subsample; when components having $b > 10$ are excluded, and using the simulation correction to the median, the median temperature of the strong sample becomes $\sim 18,000-26,000$ K. Thus, there is no evidence of a significant difference in temperature conditions between the weak and strong Mg II system populations. In addition, contrary to the conclusion of Petitjean & Bergeron (1990), we do not believe there is a significant turbulent component to the Doppler parameter.

5. DISCUSSION

6. CONCLUSION

We searched 252 HIRES and UVES quasar spectra and identified 469 Mg II $\lambda\lambda 2796, 2803$ doublets in the range $0.1 < z < 2.6$ having $\langle z \rangle = 1.18$, of which 422 were included in the final sample. We classified 180 systems as weak (having $W_r < 0.3$ Å) and 242 as strong (having $W_r \geq 0.3$ Å). We analyzed each system's absorption and kinematic properties and modeled Voigt profiles.

1. We decomposed our absorber sample using Voigt profile modeling. The VP decomposition yielded a total of 2,989 components, with an average of 2.7 and 10.3 components being recovered for the weak and strong Mg II samples, respectively. Simulations of Mg II profiles indicate that due to a systematic loss of components in the modeling process, the average actual numbers of components was ~ 3.9 and ~ 14.7 for the weak and strong Mg II samples, respectively. A linear fit to the equivalent width as a function of the number of clouds resulted in a slope of 0.116 ± 0.003 Å cloud^{-1}.

2. Fitting our VP component column density distribution over the range $12.4 \leq \log N(\mathrm{Mg\,II}) \leq 17.0$ cm^{-2} resulted in a power law slope of $\delta = 1.45 \pm 0.01$.

3. Under the assumption of thermal VP component broadening, our Doppler *b* parameter results, corrected to account for modeling artifacts, correspond to gas temperatures of $\sim 9,000-18,000$ K for the weak Mg II sample and $\sim 18,000-26,000$ K for the strong sample.

We thank Wallace Sargent, Michael Rauch, Jason Prochaska, and Charles Steidel for their contribution of spectra. We are grateful for NSF grant AST 0708210, the primary funding for this work; JLE was also supported by a three-year Aerospace Cluster Fellowship administered by the Vice Provost of Research at New Mexico State University and by a two-year New Mexico Space Grant Graduate Research Fellowship. MTM thanks the Australian Research Council for a QEII Research Fellowship (DP0877998).

REFERENCES

Churchill, C. W. 1997, Ph.D. thesis, University of California, Santa Cruz
Churchill, C. W., Vogt, S. S., & Charlton, J. C. 2003, ApJ, 125, 98
Evans, J. L., Churchill, C. W., Murphy, M. T. 2012, & Nielsen, N. M., ApJ, submitted
Petitjean, P., & Bergeron, J. 1990, A&A, 231, 309

APPENDIX

The Voigt Function

The Voigt function is the real part $u(x,y)$ of the complex probability function

$$w(x) = e^{-x^2}\left[1 + \frac{2i}{\sqrt{\pi}}\int_0^x e^{-t^2}dt\right] = e^{-x^2}\mathrm{erfc}(-iz) = u(x,y) + iv(x,y). \quad (1)$$

The Voigt profile is represented by the optical depth as a function of wavelength,

$$\tau(\lambda) = \frac{\sqrt{\pi}e^2}{m_e c^2}\frac{N f \lambda_o^2}{\Delta\lambda_D}u(x,y), \quad (2)$$

where e is the electron charge, m_e is the electron mass, c is the speed of light, N is the line of sight integrated column density, f is the atomic oscillator strength, λ_o is the transition wavelength, and $\Delta\lambda_D$ is the Doppler broadening for an ion of mass m at

temperature T:

$$\Delta\lambda_D = \frac{\lambda_o}{c}\sqrt{\frac{2kT}{m}}. \tag{3}$$

The quantity x represents the distance from the line center as a function of wavelength:

$$x = \frac{\lambda - \lambda_o}{\Delta\lambda_D}, \tag{4}$$

and y the natural width of the transition:

$$y = \frac{\lambda_o^2\Gamma}{4\pi c}\frac{1}{\Delta\lambda_D}, \tag{5}$$

where Γ is the damping constant and represents the inverse of the most probable length of time the electron will remain in the excited level.

The Doppler broadening can also be expressed in terms of the Doppler b parameter, so that $\Delta\lambda_D = [\lambda_o/c]b$. Assuming pure thermal broadening, the Doppler b parameter is $b = b_{therm} = \sqrt{2kT/m}$, where k is Boltzmann's constant, T is the temperature of the absorbing gas, and m is the mass of the absorbing species. Under this assumption, the Doppler parameters extracted through Voigt profile analysis are parameterizations of the temperature conditions under which Mg II absorption occurs. When a Gaussian turbulent component to the gas motion is assumed, the b parameter becomes $b = \sqrt{b_{therm}^2 + b_{turb}^2}$.